ResearchGate

See discussions, stats, and author profiles for this publication at: https://www.researchgate.net/publication/263990113

Grafting from Poly(3,4-ethylenedioxythiophene): A Simple Route to Versatile Electrically Addressable Surfaces

ARTICLE *in* MACROMOLECULES · JUNE 2013

Impact Factor: 5.8 · DOI: 10.1021/ma400803j

CITATIONS
12

READS
59

8 AUTHORS, INCLUDING:

Michel Nieuwoudt
University of Auckland
35 PUBLICATIONS **273** CITATIONS
SEE PROFILE

Lisa Strover
University of Auckland
6 PUBLICATIONS **47** CITATIONS
SEE PROFILE

Margaret A Brimble
University of Auckland
583 PUBLICATIONS **4,741** CITATIONS
SEE PROFILE

Jadranka Travas-Sejdic
University of Auckland
199 PUBLICATIONS **3,476** CITATIONS
SEE PROFILE

Available from: Jenny Malmstrom
Retrieved on: 27 January 2016

Macromolecules

Article

pubs.acs.org/Macromolecules

Grafting from Poly(3,4-ethylenedioxythiophene): A Simple Route to Versatile Electrically Addressable Surfaces

Jenny Malmström,*[,†,‡] Michel K Nieuwoudt,[†] Lisa T Strover,[†,‡] Alissa Hackett,[†] Olivia Laita,[†] Margaret A Brimble,[†] David E Williams,[†,‡] and Jadranka Travas-Sejdic*[,†,‡]

[†]School of Chemical Sciences, University of Auckland, Auckland, New Zealand

[‡]MacDiarmid Institute for Advanced Materials and Nanotechnology, Wellington, New Zealand

Supporting Information

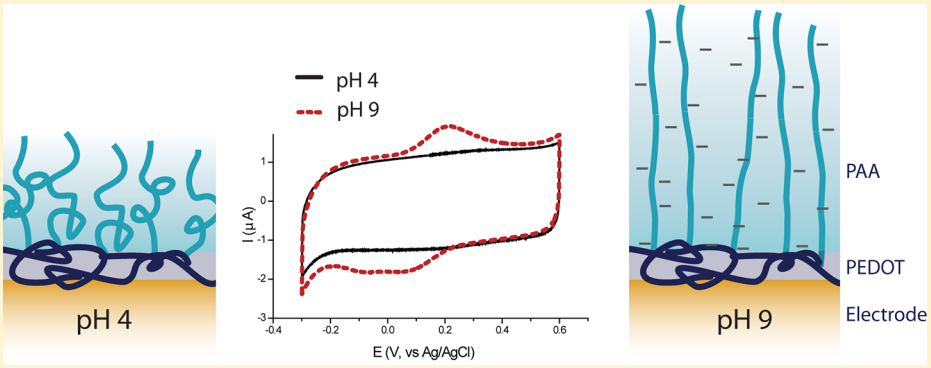

ABSTRACT: We demonstrate a simple route to versatile electrically addressable conductive polymer graft copolymer systems. The monomer of poly(3,4-ethylenedioxythiophene), one of the commercially most important conductive polymers, was modified by the addition of an ATRP-initiating site to grow brushes from. The modified monomer is easily accessible by a one-step synthesis from the commercially available 2,3-dihydrothieno[3,4-*b*][1,4]dioxin-2-yl)methanol. The modified monomer is subsequently electropolymerized onto large area gold-coated electrodes and utilized as a backbone for grafting pH-responsive poly(acrylic acid) brushes from.

INTRODUCTION

Developments within materials science have enabled the design and fabrication of advanced biointerfaces.[1−5] Stimuli-responsive surfaces are one approach to controlling the interactions of biomolecules and cells with the interface[6−9] and bring a new level of control and flexibility to cell culture. Applying electrical stimuli using a low voltage is a promising novel approach to noninvasive, switchable biointerfaces.[10,11] Electrically conducting polymers (CPs) are π-conjugated systems that can be reversibly transformed from insulating to electrically conductive states by a redox process, either chemically or electrochemically. Oxidation/reduction in CPs is accompanied by a doping/dedoping mechanism, which reversibly alters the chemical structure of CP films by balancing charges along the polymer backbone with counterions from solution.[12] In addition to their many existing uses (such as sensors, drug delivery systems, microelectronics, and photonics[13]), CPs have more recently been exploited as materials both in biomedical engineering and in interfacing electronic biomedical devices with living tissues.[1,12,14−16] The oxidation state of CP films can be varied[13] to tune their macroscopic properties; for example, surfaces patterned with CPs that switch from hydrophobic to hydrophilic upon reduction of the CP have been developed.[17] For biomedical applications, conductive poly(pyrrole) (PPy) and poly(3,4-ethylenedioxythiophene) (PEDOT) have been of particular interest due to their established biocompatibility and electroactivity in aqueous solutions.[12,16,18−20] The oxidation state of CP films has been shown to affect protein adsorption and subsequent cellular responses.[21,22] Recent developments in polymer chemistry such as controlled radical polymerization (CRP)[23] techniques provide a versatile toolbox for attaching customized polymers by "grafting to" or "grafting from" a polymer backbone, support, or surface.[24] Atom transfer radical polymerization (ATRP) and reversible addition−fragmentation chain transfer (RAFT) polymerization[23] have commonly been used to produce tailored surfaces with polymer brushes.[25] Polymer brushes based on conductive polymers have been primarily described in the literature as a means to improve or alter properties of the backbone CP, including morphology, optical or mechanical properties, and solubility.[26−35] Some CP-based brushes have also been explored as stimuli-responsive surfaces.[33,36−39] Grande et al. reported the first study on grafting of brushes from an electrochemically produced backbone;[33] however, no switching of the surface states was

Received: April 18, 2013
Revised: June 2, 2013

 © XXXX American Chemical Society dx.doi.org/10.1021/ma400803j | *Macromolecules* XXXX, XXX, XXX−XXX

Scheme 1. Grafting of Poly(acrylic acid) Brushes from the PBrEDOT Backbone (*i*: tBA, Acetone, CuBr, PMDETA, 60 °C; *ii*: 1% Methanesulfonic Acid in DCM)

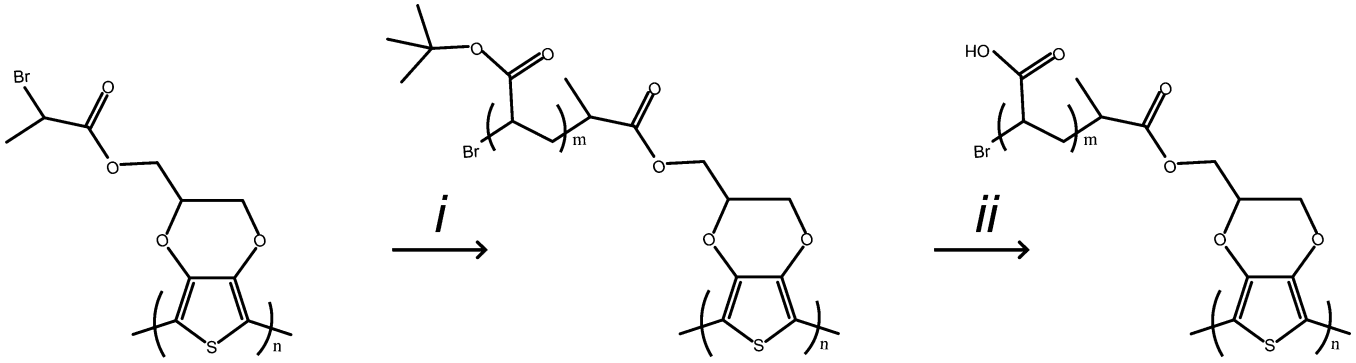

attempted. We recently reported electrochemical switching of the morphology of a poly(terthiophene)-*graft*-(polystyrene-*b*-poly(acrylic acid))[38] and ion-concentration-dependent switching of poly(pyrrole)-*graft*-poly(zwitterion) brush conformation,[36] both of which were driven by the polymer redox process.

Herein, we have modified the monomer of PEDOT, one of the most environmentally stable and commercially most important CPs, to include an ATRP-initiating site to grow brushes from. The modified monomer is easily accessible by a one-step synthesis from the commercially available 2,3-dihydrothieno[3,4-*b*][1,4]dioxin-2-yl)methanol (herein: hydroxymethyl-EDOT). The modified monomer is subsequently electropolymerized onto large area gold-coated electrodes and utlilized as a backbone for grafting pH-responsive poly(acrylic acid) brushes from.

EXPERIMENTAL SECTION

Materials. 3,4-Ethylenedioxythiophene (EDOT), hydroxymethyl-EDOT, 2-bromopropionyl bromide, 4-(dimethylamino)pyridine, *N*,*N*,*N*′,*N*″,*N*″-pentamethyldiethylenetriamine, and tetraethylammonium tetrafluoroborate were purchased from Sigma-Aldrich and used without further purification. Sodium chloride (Scharlau, reagent grade) was used as received. Copper(I) bromide was purified by stirring in glacial acetic acid overnight, washed with ethanol and then diethyl ether, and dried under vacuum.[40] *tert*-Butyl acrylate (Sigma) was extracted three times with 5% NaOH and three times with water. The organic layer was dried with $MgSO_4$, filtered and distilled under vacuum at 60 °C,[40] and stored under nitrogen in a freezer until use. All solvents were used as received unless otherwise stated. Gold-coated glass slides were prepared by evaporation of a chromium adhesion layer (1.2×10^{-4} Torr, 21 A, 10 s), directly followed by gold evaporation (1.2×10^{-4} Torr, 20 A, 2.50 s) (JEOS metal evaporator). Buffers used were prepared with Milli-Q water and filtered through a 0.2 μm pore filter prior to use in SPR experiments. The buffers used were TBS (25 mM TRIS (tris(hydroxymethyl)aminomethane), NaCl 137 mM, KCl 2.7 mM, pH 7.4) and PBS (phosphate buffered saline, Sigma) at quarter strength (ionic strength 50 mM) adjusted to pH 4 or 9.

Synthesis of (3,4-Ethylenedioxythiophene)methyl 2-Bromopropanoate. The synthesis of (3,4-ethylenedioxythiophene)methyl 2-bromopropanoate (BrEDOT) was as follows: 2-Bromopropionyl bromide (2.32 mmol, 244 μL) was added dropwise under nitrogen to a stirred flask of dichloromethane (9.2 mL), hydroxymethyl-EDOT (1.16 mmol, 200 mg), 4-(dimethylamino)pyridine (0.872 mmol, 106 mg), and triethylamine (3.48 mmol, 486 μL) at 0 °C. The reaction was stirred for 3 h at room temperature, washed with brine (1 × 20 mL), 10 mM $NaHCO_3$ (1 × 20 mL) and deionized water (2 × 20 mL), and dried over anhydrous magnesium sulfate. The solvent was removed *in vacuo* and the residue purified by silica gel column chromatography (hexane/ethyl acetate 3:1), affording monomer BrEDOT as a pale yellow oil (223 mg, 0.726 mmol, 63%). ^{1}H NMR (400 MHz, $CDCl_3$): *d* 1.83 (3H, d, CH_3), 4.04−4.47 (6H, m), 6.35 (2H, s, Ar).

Electrochemical Polymerization. Electrochemical polymerization was performed by cyclic voltammetry (CV) in a three-electrode cell with a gold-coated glass substrate (~1 cm^2) or 1 mm gold disk electrode as the working electrode, platinum wire or mesh counter electrode, and an Ag/AgCl reference electrode. The disk working electrode was polished with alumina and electrochemically cleaned by 10 cycles between −0.2 and 1.5 V in 0.05 M H_2SO_4, while the gold-coated glass substrates were cleaned by sonication for 5 min each in acetone, ethanol, and MQ water and dried using nitrogen prior to use. Polymerization parameters were controlled and monitored using a CH Instruments model 650 potentiostat. Polymerization of BrEDOT, EDOT, or a mixture thereof took place from a total monomer concentration of 0.02 M in propylene carbonate (PC) with 0.1 M tetraethylammonium tetrafluoroborate ($TEABF_4$). The polymer films were grown by cyclic voltammetry (CV) (−0.6 to 1.4 V, 0.1 V/s, 10 cycles for pure PEDOT films and 20 cycles for PBrEDOT films or copolymerized films). Films used for subsequent grafting from reactions were polymerized using only three cycles for SPR samples and seven cycles for samples used for other characterization. Films were characterized electrochemically by CV in monomer-free solution (PC, $TEABF_4$) as well as in acetonitrile/$TEABF_4$ and TBS (aqueous buffer solution with NaCl as electrolyte), using the same electrochemical cell setup as for the polymerization.

Grafting of Poly(acrylic acid) Brushes from CP Backbone. Poly(acrylic acid) (PAA) brushes were produced by grafting of *tert*-butyl acrylate (tBA) by surface-initiated ATRP (Scheme 1). tBA (10 mL) and acetone (p.a, 15 mL) were added to a flask and bubbled with nitrogen for at least 1 h. The tBA and acetone mixture was then frozen in liquid nitrogen, and CuBr (50 mg) added under a nitrogen atmosphere. The flask was then sealed and defrosted. PMDETA was added by syringe (70 μL), and the mixture was stirred at 60 °C for ~1 h under nitrogen. The samples with the CP films (PBrEDOT or PEDOT as negative control) were dried from acetonitrile and placed in small round-bottom flasks that were sealed, evacuated, and then backfilled with nitrogen. The solution with tBA and catalyst complex was added to the flasks with samples and placed in the water bath at 60 °C with mild agitation (shaking at 60 rpm) for the desired time (2−20 h). Samples were rinsed with acetone and analyzed with the brushes in either tBA form or subjected to acid hydrolyis of the *tert*-butyl group to yield the PAA brushes. For acid hydrolysis, the samples were rinsed with tetrahydrofuran for 5 min, followed by rinsing in acetone and dichloromethane (DCM), and were agitated for 15 min in a beaker filled with 10 mL of DCM and 0.1 mL of methanesulfonic acid. Samples were then rinsed with DCM and ethanol.

Characterization. Raman spectra were recorded in backscattered mode using the Renishaw System 1000 Raman microprobe with Grams spectroscopic software. Excitation at 785 nm at 26 mW was provided by a Renishaw solid state diode laser, used with a 1200 grooves/mm grating, while the 488 nm excitation line was provided by an air-cooled Spectra-Physics argon ion laser at 30 mW, with a 2400

dx.doi.org/10.1021/ma400803j | *Macromolecules* XXXX, XXX, XXX−XXX

grooves/mm grating. Power at the sample for each laser was reduced to 0.1 mW to prevent thermal degradation. Resolution was 6 cm^{-1} and entrance slit 50 μm. HNF filters were used to remove Rayleigh scattered light below 200 cm^{-1}. FTIR spectra were recorded in ATR mode using the Smart Orbit ATR accessory with Ge crystal of the Nicolet 8700 Thermo Electron FTIR spectrometer at resolution 4 cm^{-1}. The spectra were processed and corrected for distortion by the Ge crystal using the OMNIC spectroscopic software. The X-ray photoelectron spectroscopy (XPS) data were collected on a Kratos Axis UltraDLD equipped with a hemispherical electron energy analyzer. Spectra were excited using monochromatic Al Kα X-rays (1486.69 eV) with the X-ray source operating at 150 W. Survey scans were collected with a 160 eV pass energy, while core level scans were collected with a pass energy of 20 eV. The analysis chamber was at pressures in the 10^{-9} Torr range throughout the data collection. Data analysis was performed using CasaXPS software. Shirley backgrounds were used in the peak fitting. Quantification of survey scans utilized relative sensitivity factors supplied with the instrument. Core level data were fitted using Gaussian−Lorentzian peaks (30% Lorentzian). The number of carboxylic groups present on the PAA grafted films was estimated by a toluidine blue (TB) assay according to the method reported by Sano et al.[5] Grafted samples (thin CP films electropolymerized and grafted in accordance to SPR samples), ungrafted controls (electropolymerized using six segments), and bare substrate controls were all prepared on 0.36 cm^2 gold-coated wafer pieces. The result is an average of five samples (from three independently prepared films) or three control samples. Atomic force microscopy (AFM) was performed (Digital Instruments, Nanoscope III) in air, using tapping mode with NSG 01 probes (resonance frequency ≈140 kHz) from NT-MDT (Russia). Films were characterized electrochemically by CV between −0.3 and 0.6 V (using a model CH650 potentiostat or BioLogic SP-300 potentiostat). Surface plasmon resonance (SPR) (BioNavis, Finland) was used to follow the swelling and collapse of the grafted PAA brushes. The SPR was equipped either with a dual channel flow cell (controlled by a 12 port injection valve) or with an electrochemical cell. The electrochemical cell was equipped with a coiled platinum wire (covering a large area opposing the working electrode, which is the SPR chip itself) as the counter electrode and a silver wire as the reference electrode. For SPR, PBrEDOT films were electropolymerized extremely thinly (6−20 nm) and homogenously using a homemade polymerization chamber made of polydimethylsiloxane (PDMS) with stainless steel as the counter electrode and an Ag/AgCl wire as the reference electrode. During the SPR experiments, the films were either exposed to different pH liquids (unbuffered MQ water, adjusted to basic (≈10) or acidic (≈4) pH) using the microfluidic flow cell. Unbuffered solutions were used in order to allow for a low ionic strength. Using the electrochemical cell, a range of potentials were applied to the film. The solution in the electrochemical cell was quarter-strength PBS (ionic strength of 50 mM) adjusted to pH 9 or pH 4.

RESULTS AND DISCUSSION

Synthesis of CP Films with ATRP Initiator. For many applications of stimuli-responsive surfaces, such as for switchable cell adhesion, a large surface area is needed for both a meaningful experimental readout and particularly for future commercial applications. Here, we present a one-step simple route to an ATRP-initiating site functionalized EDOT monomer from a commercially available starting material. EDOT makes an ideal starting point for derivatization, as it is well characterized in terms of biocompatibility and is electroactive in aqueous solutions (a prerequisite for successful electrically switchable surfaces in biological environments). The ease of the monomer synthesis presented here, compared to several other promising termonomers modified with ATRP sites,[38,39] makes this an advantageous candidate for surface-grafted electrically accessible molecular brushes. Electropolymerization of CPs is furthermore a simple route to surface adhered CP films. The BrEDOT monomer was subjected to a range of polymerization conditions (different solvents, electrolyte salts, and working electrode materials). Gold is a versatile working electrode material as it is relatively cheap and easy to deposit and pattern by standard lithographic methods; therefore, gold film deposited on microscopic glass was chosen here as preferred substrate. Figure 1 shows polymerization CVs

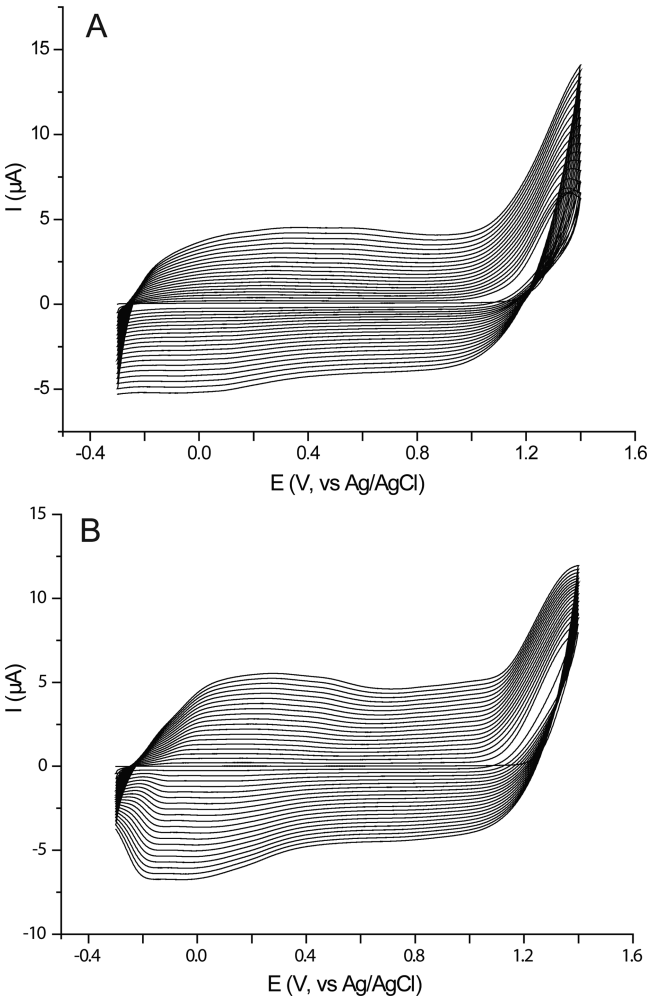

Figure 1. Polymerization of (A) EDOT and (B) (3,4-ethylenedioxythiophene)methyl 2-bromopropanoate) from solutions containing 0.02 M monomer and 0.1 M $TEABF_4$ in PC onto a 1 mm diameter gold disk electrode, 10 cycles for EDOT and 20 cycles for BrEDOT.

of BrEDOT and EDOT on a standard 1 mm gold disk electrode, obtained under optimized electropolymerization conditions particularly with respect to film adhesion to the electrodes. After initial characterization, the subsequent films were prepared on larger gold-coated glass substrates.

For both monomers, successful polymer growth is illustrated by the increase of the amplitude of the current upon successive cycling. Several clear differences can be seen in the polymerization CVs of EDOT (Figure 1A) and BrEDOT (Figure 1B). First it is evident that the onset of polymerization occurs at a lower potential for EDOT (1.1 V) than for BrEDOT (1.2 V). EDOT also polymerizes faster with higher current densities observed for each cycle compared to BrEDOT. There are also additional peaks showing up in the spectra for the polymer formed from BrEDOT. The classical broad oxidation peak for

dx.doi.org/10.1021/ma400803j | Macromolecules XXXX, XXX, XXX−XXX

PEDOT is seen here at 0.3 V (with corresponding reduction peak at 0.1 V). However, for PBrEDOT the peak is distinctly split up into two (at 0.2 and 0.5 V, with reduction peaks at −0.2 and 0 V, respectively). This may relate to a bimodal distribution of molecular weight of the polymer or a small proportion of polymeric chains being branched or cross-linked.[41]

The films grown on the gold disk electrode were characterized by CV in PC/TEABF$_4$ (Figure 2) or acetonitrile

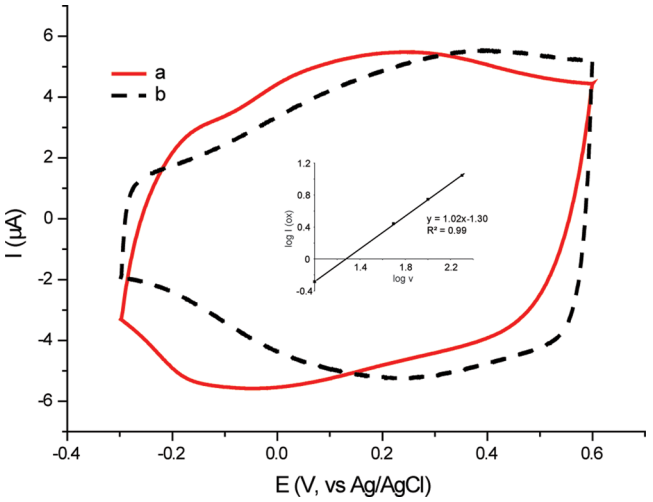

Figure 2. Characterization of a PBrEDOT film on 1 mm Au disk electrode by CVs in (a) PC/0.1 M TEABF$_4$ or (b) TBS buffer, scan rate 0.1 V/s. Inset illustrates the proportional dependence of the oxidation peak current on the scan rate.

(Figure S1). Furthermore, CVs were recorded in aqueous buffer solution, namely tris buffered saline (TBS), a physiological buffer at pH 7.4 with NaCl as the primary electrolyte. The CVs (Figure 2) clearly display a capacitive behavior as expected for EDOT-based CPs.[41−46] In both of the organic solvents (acetonitrile and PC), the polymer is readily oxidized and reduced. In PC/TEABF$_4$ the polymer is oxidized at a potential of about 0.2 V and reduced at −0.1 V. Again, there appears to be several redox peaks overlaid, which may relate to bimodal chain lengths or network formation/cross-linking of the film.[41] The corresponding CVs for PEDOT are presented in Figure S2 and show similar features, with PEDOT being oxidized at slightly higher potential in PC than PBrEDOT (0.35 V ox and 0.1 V red). The PEDOT film behaves as a largely potential independent capacitor in the investigated solvents, whereas the BrEDOT film displays a potential dependence of the capacitance where the potential dependence in turn depends on the solvent and ions present. The CVs in physiological aqueous buffer (TBS) importantly show that the PBrEDOT films are electroactive in aqueous solutions. There is a shift to higher oxidation potentials in the aqueous solution. This extra energy needed to oxidize the polymer in aqueous solution relates to the different solubility of the polymer in water and PC. The reduced solubility of the polymer in the aqueous solution is expected to lead to a more compact film that hinders charge transfer during the electrochemical processes.[47] CVs were also obtained using scan rates of 0.01, 0.05, and 0.2 V/s. The inset in Figure 2 illustrates the linear dependence of the logarithm of the peak oxidation current on the scan rate with a slope of 1. CVs for PC/TEABF$_4$ are presented here (Figure S2 shows the corresponding relationship for PEDOT), and the same behavior was seen in acetonitrile and TBS (data not shown). Such a linear relationship is consistent with the capacitive behavior of the films. To control the density of the functional groups at the surface, BrEDOT and EDOT were copolymerized, and the produced polymers were characterized by XPS. As BrEDOT polymerizes at slightly higher potentials than EDOT, it is expected to be incorporated into a copolymer to a lower extent than its composition in the feed solution. The individual polymers' voltammograms can be used to obtain a basic indication for the copolymerization process as the voltammograms differ for the two polymers (Figure 1). To quantify the copolymer composition, XPS was performed and the Br/S ratio of the samples analyzed. Figure 3 shows the relationship between the monomer feed ratio and the copolymer composition, expressed as Br/S ratio.

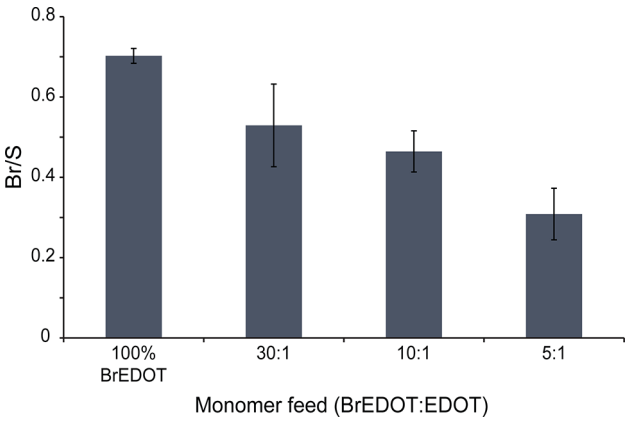

Figure 3. XPS data to quantify the copolymerization of BrEDOT and EDOT. The graph shows the Br/S ratio in the copolymer for each monomer feed.

Upon analysis of the XPS data (table of elemental composition in Table S1), it is evident that copolymers of the two monomers are produced. The theoretical Br/S ratio for pure PBrEDOT is 1, and the measured ratio is 0.7 (Figure 3). Some variation from the expected theoretical value can be attributed to factors related to the instrument and the sensitivity factors used and orientation of the molecules at the surface. However, in this case, the measured ratio is low enough to indicate that some portion of the functionalized monomer does not bear a bromine atom. This could relate to contamination of starting material (hydroxymethyl-EDOT) from the monomer synthesis or that some bromine is lost during the electropolymerization. However, the initiator density on the surface remains much higher (≥24 initiator sites/nm^2 projected area estimated from a 12 nm thick film with a density of 1.45 g/cm^3) than the maximum grafting density expected from literature (≈1 chain/nm^2).[48] The full elemental table from these experiments is presented in the Supporting Information. The high-resolution scan of the S 2p region of the PBrEDOT sample reveals several different sulfur species (Figure S3, for all high-resolution scans and assignments). These have been attributed to the neutral and charged thiophenes.[49−51] A small peak is also seen at high binding energies, possibly relating to oxidized sulfur species. By examining the peak areas, it can be seen that 24% of the thiophene sulfurs are charged/doped. The samples were reduced before XPS, and the low level of fluorine remaining (the ratio of F/S is as low as 0.02) shows that the

dx.doi.org/10.1021/ma400803j | Macromolecules XXXX, XXX, XXX−XXX

medium size anion BF_4^- is readily expelled from the film upon reduction. The charged sulfur is most likely due to oxidation occurring upon exposure to the oxygen in air. Traces of nitrogen in the BrEDOT containing films indicate involvement of the tetraethylammonium cation in the doping process of the modified film (Table S3).

Raman and FTIR Spectra. Raman and FTIR spectra of PEDOT,[52−54] and its C_{14}-alkyl derivative,[53,54] have been reported using 457.9,[54] 514.5,[53,54] 676.4,[54] 785,[52] and 1064 nm[53,54] excitation. In these studies Raman and FTIR spectra of the PEDOT have been recorded in situ during oxidation and reduction, during which spectral changes were observed with oxidation, particularly in the Raman spectra. In addition, differences were observed when different excitation lines were used. In this study, the Raman spectra of PBrEDOT and PEDOT in both the neutral (reduced) and charged (oxidized) forms were compared, using two different excitation wavelengths in the near-infrared (785 nm) and visible (488 nm) regions. Different vibrational modes have been found to be selectively enhanced by the use of different wavelengths due to near-resonance effects,[53] so the use of these two wavelengths was deemed useful to provide more information on the electronic modification of the polymer with oxidation. FTIR spectra were also recorded of PEDOT and PBrEDOT. To our best knowledge, no vibrational spectra of PBrEDOT have yet been reported in the literature. IR and Raman spectra of PEDOT and PBrEDOT were compared, and changes in the Raman spectra were examined upon oxidation and under different excitation wavelengths. As expected, significant differences were found in the spectra upon oxidation of the polymer films, as well as between spectra recorded using 488 and 785 nm excitation lines, demonstrating the modification of the electronic distribution along the polymer chain.

The Raman spectra between 1200 and 1600 cm^{-1} of the reduced and oxidized forms of PEDOT and PBrEDOT which were recorded using the 785 and 488 nm laser are given in Figures 4A and 4B, respectively. The bands are complex and consist of a number of components which are due to C−C and C═C stretching vibrations. The complexity of these bands is probably due to the presence of nonplanar structures with small but different helical angles and their intermolecular interactions,[55] which makes it difficult to resolve and assign the bands. However, it is apparent that different modes are enhanced with the 488 and 785 nm excitations providing useful information about the changes occurring upon oxidation and the effect of the Br butyl acetate group.

With the 488 nm excitation, the Raman modes between 1410 and 1575 cm^{-1} are more intense compared to the 785 nm excitation. This is due to a near-resonance enhancement effect, as the absorption spectrum of PEDOT shows a broad, intense optical absorption band with a maximum at 600 nm due to $\pi\rightarrow\pi^*$ transitions of the conjugated backbone.[53] The 488 nm line lies on the shoulder of this band which is close enough to afford a near-resonance enhancement of the bands associated with this transition. As seen in PEDOT in Figure 4, the mode at 1433 cm^{-1} (C_α═C_β(−O) symmetric stretch[52−54]) is blue-shifted by 18 cm^{-1} to 1451 cm^{-1} upon oxidation, while the C═C asymmetric stretch mode at 1519 cm^{-1} undergoes a red-shift to 1508 cm^{-1}. In PBrEDOT, the symmetric C_α═C_β(−O) stretch[52−54] occurs at a higher frequency (1444 cm^{-1}) and is blue-shifted by only 2 cm^{-1} upon oxidation, while the C═C asymmetric stretch mode also occurs at 1519 cm^{-1} and undergoes the same shift as for PEDOT. The vibrational mode

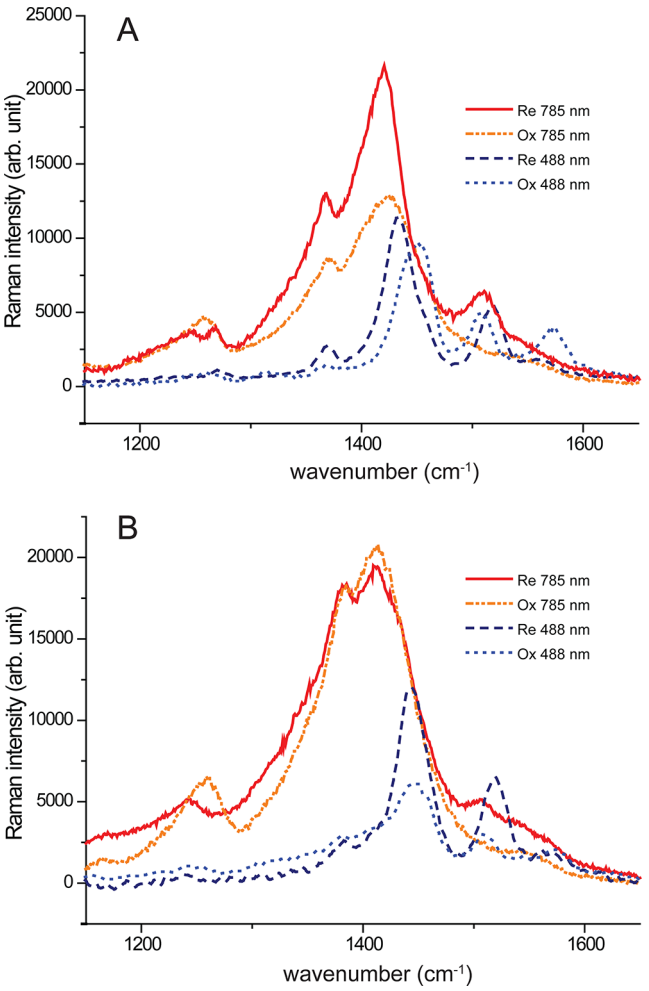

Figure 4. Comparison of Raman spectra recorded with 488 and 785 nm laser in oxidized and reduced forms. Spectra for PEDOT in (A) and PBrEDOT in (B).

at 1562 cm^{-1} also behaves similarly for PEDOT and PBrEDOT, undergoing a blue-shift of 12 cm^{-1} upon oxidation. No assignment could be found in the literature for this mode; however, both its enhancement at this excitation and blue-shift with oxidation suggest it is associated with the C_α═C_β(−O) symmetric stretch. The blue-shift of the 1562 and 1433 cm^{-1} modes indicate an increase in the bond force constant due to delocalization of charge upon oxidation, which is reduced in the case of the PBrEDOT—probably as a result of the charge being distributed along the Br butyl acetate side chain (referred to as the ATRP-initiating site). Similarly, the C_α−C_α' inter-ring stretch mode occurring at 1247 cm^{-1} for PEDOT and PBrEDOT is significantly blue-shifted by 10−17 cm^{-1} upon oxidation, although for PBrEDOT this mode is lowered by 5 cm^{-1} by the substitution of the ATRP-initiating site. This mode is not enhanced by the 488 nm as it is not associated with $\pi\rightarrow\pi^*$ transitions of the conjugated backbone and is more intense with the 785 nm laser. Other modes that are more intense with the 785 nm excitation are the bands at 1425 and 1415 cm^{-1} (symmetric C_α═C_β stretch[52−54]), 1370 cm^{-1} (C_β−C_β stretch[52,54]), 992 cm^{-1} (oxyethylene ring deformation,[52−54] C_α−S stretch[55]), and 445 cm^{-1} (out-of-plane ring deformations[55]). The substitution of PEDOT with the ATRP-initiating site results in a red-shift of the out-of-plane ring deformation mode around 448 cm^{-1}, the oxyethylene ring deformation

dx.doi.org/10.1021/ma400803j | Macromolecules XXXX, XXX, XXX−XXX

around 1102 cm^{-1}, and the oxyethylene ring deformation[52−54] with C_α−S stretch[55] at 991 cm^{-1}. However, the mode at 575 cm^{-1} which is due to both oxyethylene ring deformation modes and C_β−H, C_α−H bending undergoes a blue-shift of around 13 cm^{-1}. The C−S−C ring deformations at around 700 cm^{-1} are not affected by the presence of the ATRP-initiating site. The full Raman spectra and band assignments are available in the Supporting Information (Figures S4, S5 and Table S2).

The FTIR spectra of PEDOT and Br-PEDOT films are compared in Figure 5. The FTIR spectra show clearly the C═O stretch mode of the acetyl group of the ATRP-initiating site in the PBrEDOT polymer, which occurs at 1744 cm^{-1}. Overall, the spectra of the PEDOT and PBrEDOT films are similar, with additional bands observed in the PBrEDOT spectrum at 1494, 1437, 1316, 1298, and 1190, 1160, 1099, 1031, and 974 cm^{-1}, in addition to that at 1744 cm^{-1} due to the C═O stretch mode. A significant decrease in intensity is observed in the vibration at 1059 cm^{-1} (C−O−C deformation,[52−54] Cβ-H, Cα-H bending), which indicates changes to the oxyethylene ring, as also seen in the Raman spectra. Full band assignments are available in Table S3.

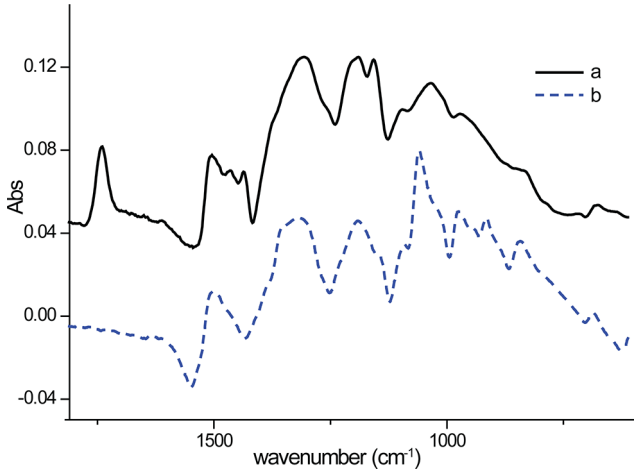

Figure 5. Comparison of FTIR spectra of PBrEDOT (a) and PEDOT (b).

The FTIR and Raman spectra have established the presence of the ATRP initiating site in the polymer. The changes in selected bands in the Raman spectra of PBrEDOT upon oxidation (Figure 4) show that the polymer indeed undergoes changes to the electronic distribution upon changes in the oxidation state. The changes are not as marked as for PEDOT, which is attributed to the steric hindrance of the added Br-acetyl group. In addition, the bands showed broadening compared to PEDOT, which was attributed to network formation or polydispersity in the film, as suggested also by the presence of additional peaks in the CVs (Figures 1 and 2). The use of more than one excitation wavelength highlighted the significant frequency shifts accompanying changes in the electronic structure upon oxidation of this polymer. The significant changes between the spectra of PEDOT and PBrEDOT mainly affected the oxyethylene ring, while the significant shift of the inter-ring stretch modes upon oxidation indicated that PBrEDOT is well conjugated in the oxidized form.

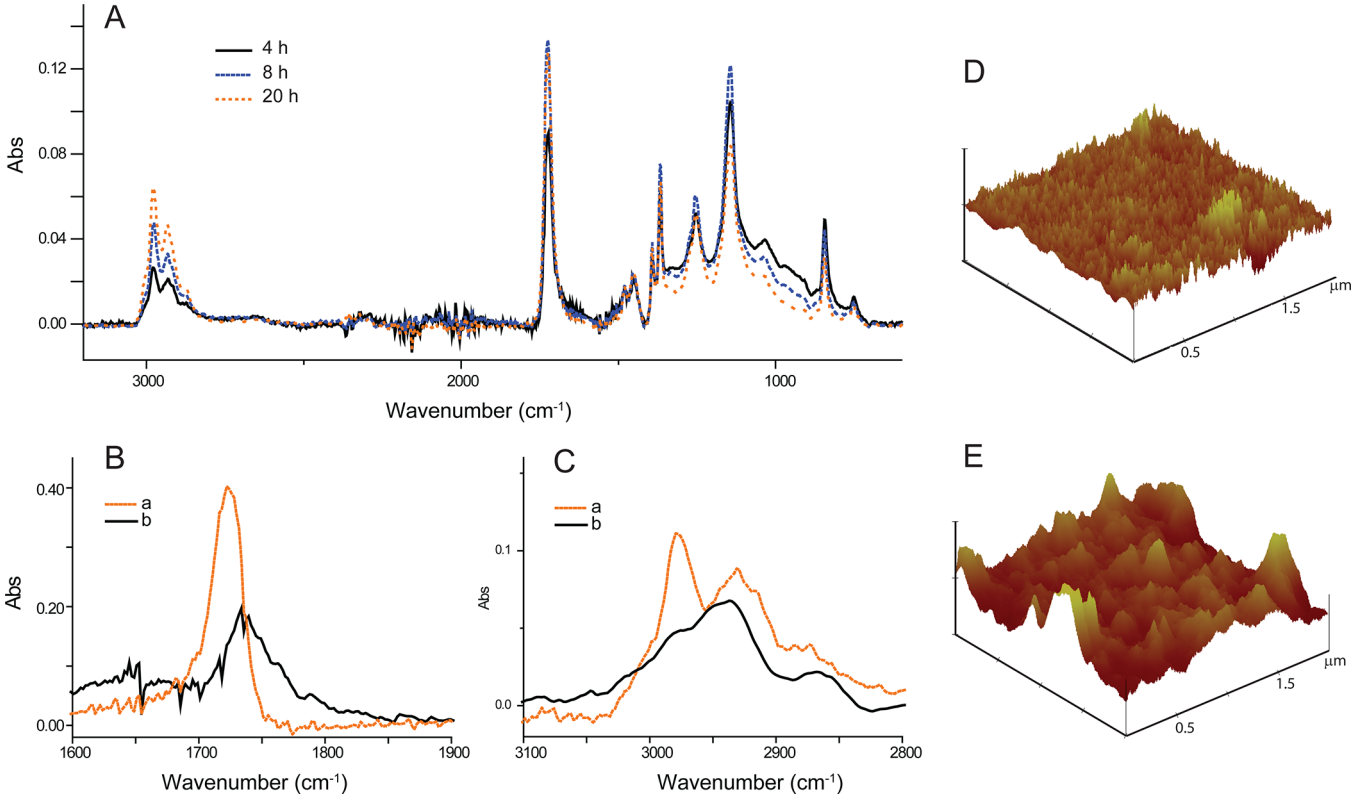

Figure 6. (A) FT-IR confirming grafting of tBA. (B) FT-IR of acid region and (C) C−C stretch region of PBrEDOT-*g*-tBA (a) and PBrEDOT-*g*-$PAA^{(-)}$ (b) grafted under similar conditions. (D, E) AFM height images of 2 μm scans of PBrEDOT before (D) and after grafting of tBA and conversion to PAA (E). The height scale is 20 nm in both images.

dx.doi.org/10.1021/ma400803j | *Macromolecules* XXXX, XXX, XXX−XXX

Grafting from PBrEDOT Films. To verify that the polymer is suitable for grafting from, we grew polystyrene and *tert*-butyl acrylate from the PBrEDOT films by surface-initiated ATRP. FT-IR spectra of the polystyrene grafted film are presented in Figure S6; Figure 6 shows FT-IR spectra of films grafted with tBA for various times. The clear time-dependent growth of the characteristic tBA C−C stretch peaks at 2800−3100 cm^{-1} and the ester C═O stretch at around 1700 cm^{-1} verifies successful grafting (spectra normalized to peak at 1450 cm^{-1}). For further film analyses, the grafting time was kept short in order to make films well adherent to the substrates as some delamination often started to occur with longer grating times. This is likely due to the solubility of the tBA brushes under the grafting conditions, effectively pulling the film off the substrate. The longer the brushes, the higher is this "solvation force".

In order to make the grafted brushes pH responsive, the *tert*-butyl group was hydrolyzed to yield poly(acrylic acid) brushes. Figure 6 shows FT-IR spectra of the carboxylic acid region (B) and the C−C stretch region (C) of the film before and after conversion to poly(acrylic acid). The FT-IR spectrum of the converted film was taken after the sample had been exposed to MQ-water with ≈pH 8; thus, the brushes are expected to be deprotonated and swollen. The C═O peak shifts from 1722 cm^{-1} for PBrEDOT-*g*-tBA to 1735 cm^{-1} for PBrEDOT-*g*-$PAA^{(-)}$, in excellent agreement with the literature (poly(acrylate) reference spectrum in Figure S7). Furthermore, a shift of the C−C components from mainly methyl to mainly ethyl is also evident after the conversion.

Qualitatively, successful grating and subsequent conversion to PAA could also be confirmed through water contact angle measurements where an ungrafted film presented an average contact angle of ∼55°, which changed moderately to 65° after grafting with the tBA brushes, but was reduced to around 35° after the acid hydrolysis of the *tert*-butyl group. Surface derivatization could aslo be confirmed by binding the carboxylic groups of the PBrEDOT-*g*-PAA samples to toluidine blue (TB) under basic conditions. The bound TB was subsequently released and the absorbance thereof measured. A significant amount of carboxylic groups was confirmed (742 ± 79 carboxylic groups/nm^2 for PBrEDOT-*g*-PAA as compared to 81 ± 25 and 40 ± 7 carboxylic groups/nm^2 for the ungrafted control and bare substrates, respectively). The relatively high TB binding to the control samples is attributed to entrapment within the porous CP film and to the rough backside of the wafers. It is noteworthy that the CP films are rough and exhibit a larger surface area than the projected area quoted here for comparison. Atomic force microscopy (AFM) images in Figure 6 clearly display this surface roughness and further support successful grafting. Figures 6D and 6E show representative 2 μm scans of PBrEDOT and PBrEDOT-*g*-PAA, respectively. A very clear change in morphology is seen after grafting of polymer brushes with the features increasing in size both laterally and vertically with the addition of the polymer brushes.

Electrochemical Characterization of PBrEDOT-*g*-PAA. It is interesting to see how grafting of the side chains affects the redox properties of the conductive polymer film, investigated here by cyclic voltammetry. As the PAA brushes are well-known to be pH-responsive,[56−58] we investigated the films at pH 4 where the brushes are expected to be fully protonated, uncharged, and collapsed and at pH 9 where they are expected to be fully deprotonated, charged, and extended.[48,58−61] The pK_a of surface-bound polymer brushes is known to be quite different than that of solution material; it varies within the layer and depends on factors such as grafting density and layer thickness.[56] For PAA in bulk, pK_a values of about 6.5 has been reported while the outermost surface of a PAA layer grafted from a planar surface was experimentally determined to have a pK_a as low as 4.4 by Dong et al.[56] The cyclic voltammagrams shown in Figure 7A reveal drastic pH-dependent changes for

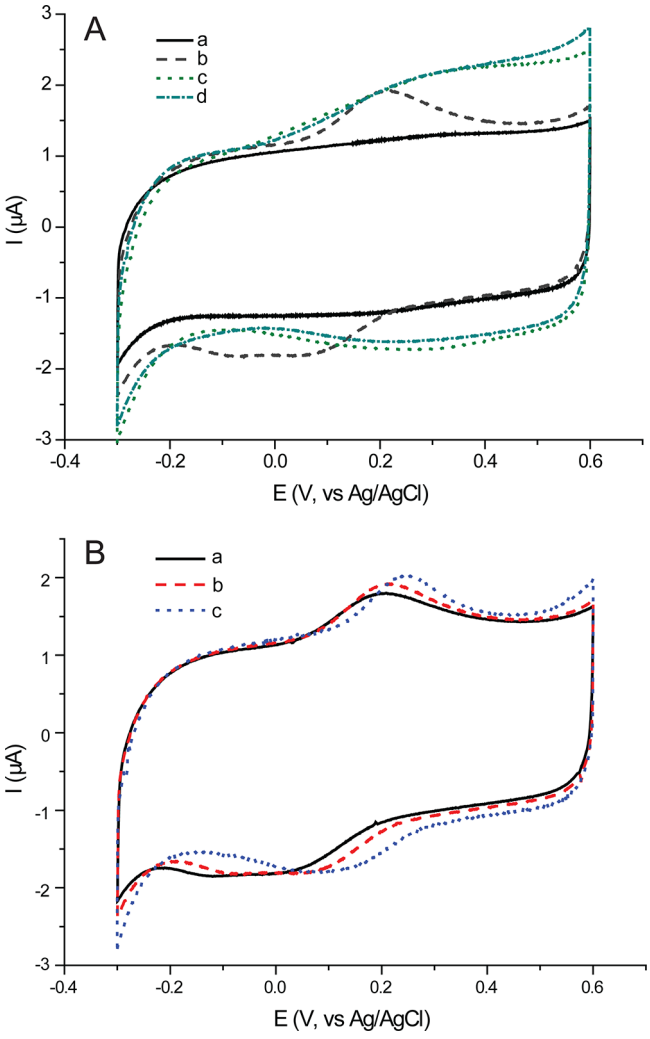

Figure 7. (A) CVs of PBrEDOT-*g*-PAA (a: pH 4; b: pH 9) and the control PBrEDOT (c: pH 4; d: pH 9) at acidic and basic pH with 100 mM of NaCl. (B) CVs of PBrEDOT-*g*-PAA at pH 9 with increasing concentration of NaCl (a: 50 mM; b: 0.1 M; c: 0.5 M).

the PBrEDOT-*g*-PAA film, while the ungrafted control remains rather unaffected by the pH. As previously illustrated in Figure 2, the PBrEDOT exhibits a rather broad oxidation peak in aqueous solution (here MQ set to pH 4 or 9, without added buffer component, and 100 mM added NaCl). The broad oxidation peak of PBrEDOT occurs at ∼0.3 V with the corresponding reduction at only slighty lower potential. The reduction peak is broad and appears to be two peaks overlapping. For PBrEDOT-*g*-PAA at pH 9 (extended charged brushes), a much more defined oxidation peak occurs at 0.2 V now with the clearly separated reduction peaks centered around approximately 0.05 V. When the pH is changed to pH 4, the redox peaks vanish and the film acts as a capacitor. This can be understood in terms of adding a thin insulating layer on top of the CP film, in this case the collapsed PAA brushes. The much

dx.doi.org/10.1021/ma400803j | *Macromolecules* XXXX, XXX, XXX−XXX

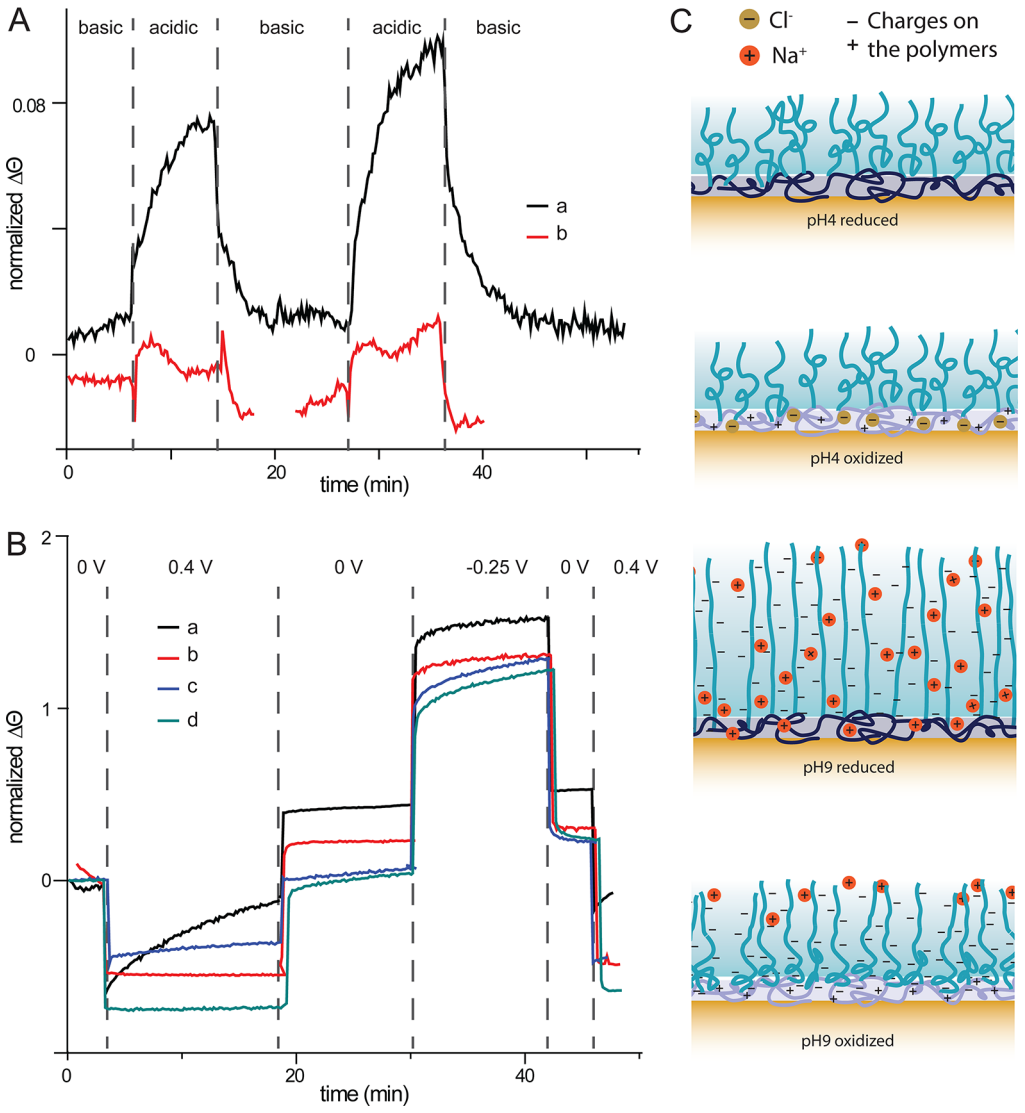

Figure 8. SPR data following the change in resonant angle over time. (A) Response upon change from water of basic pH (≈10) to water of acidic pH (≈4) for (a) PBrEDOT-*g*-PAA and (b) PBrEDOT. (B) Response of the polymers to changes in oxidation state under basic or acidic conditions (a: PBrEDOT-*g*-PAA at pH 9; b: PBrEDOT-*g*-PAA at pH 4; c: PBrEDOT at pH 9; and d: PBrEDOT at pH 4). (C) Illustration of proposed changes to the polymeric layers.

improved redox behavior for PBrEDOT-*g*-PAA at pH 9 compared to PBrEDOT deserves some further attention. The redox peaks are more defined and occur at a lower potential. This means it is easier to oxidize the PBrEDOT-*g*-PAA film and that the redox processes occur more evenly across the sample. We explain this behavior as a solvation effect where the charged water-soluble PAA brushes solvate the CP film well, which causes it to be more readily oxidized and reduced. One of the major drawbacks of CPs are their low solubility in water, which often makes them unsuitable for biological applications.[47] Here we demonstrated a route toward CP materials with improved electrochemisty in aqueous environments. However, the oxidation peak of PBrEDOT-*g*-PAA is even more defined than that of PBrEDOT in PC/TEABF$_4$ (Figure 2). As PBrEDOT is expected to be more soluble in propylene carbonate than water, the effect seen for PBrEDOT-*g*-PAA (pH 9) is likely more than purely a solvation effect. The grafted charged brushes may also be involved in the doping process,[37,41,62,63] and the diffusion-unrelated proximity of these charges to the CP may serve to make the redox process more uniform. Ali et al.[64] demonstrated similar, but less extreme, pH-dependent effects on the CVs of P(EDOT-COOH). They attributed the increased peak current and larger separation between anodic and cathodic peak potentials, occurring at higher pH, to more localized and kinetically restrained cationic charge carriers. Similar self-doping effects has also been reported for sulfonated EDOT.[65]

Surface-grafted PAA brushes have been shown to be sensitive to not only pH but also the concentration of salt in the solution.[37,48,60,66,67] Literature shows some discrepancies, however, with different dependence on the salt concentration found. This has been attributed to differences in grafting densities and layer thicknesses.[66] Wu et al.[48] and Gong et al.[60] present experimental data followed by theory and calculations. The dependence of PAA brushes on salt is complicated by the pH dependence of the brushes. At the fully dissociated state though, the brushes behave as a strong polyelectrolyte, leaving the local pH in the brush unaffected by ionic strength.[60] At pH 10, Gong et al. showed an extension of the layer with increasing salt concentration until about 0.2 M, after which the thickness

dx.doi.org/10.1021/ma400803j | *Macromolecules* XXXX, XXX, XXX–XXX

of the layer decreased moderately. This was explained by counterion condensation followed by charge screening effects.[60] For our PBrEDOT-*g*-PAA surfaces with the brushes in the extended state (pH 9), one can anticipate a change in layer thickness depending on the salt concentration. We therefore recorded the CVs with progressively higher salt concentrations as seen in Figure 7B (figure with all tested salt concentrations, 1 mM to 0.9 M, in Figure S8). It was seen that the oxidation peak shifted to slightly higher potential with increasing salt concentrations, which is consistent with a cation flux in the film and thus supporting the hypothesis of a partially self-doped polymer. The reduction peaks also shifted to higher potentials, and the second component of the reduction diminished with increasing salt concentration. It appears that the redox process becomes more reversible with increasing salt concentration, consistent with less restrained charge carriers, which relates to the screening effect of the salt on the PAA charges. No such effect of salt concentration was seen in the CVs of PBrEDOT-*g*-PAA at pH 4 or for the ungrafted PBrEDOT at either pH (data not shown). A shift of the oxidation peak to a higher potential may relate to the same effect of charge screening where PAA brushes are progressively less solvated. The gradual disappearance of the second reduction peak may relate to a switch from a self-doping process to a Cl^- doping process, which would be anticipated by both the expected compaction of the layer as well as the abundance of ions in the bulk solution at the higher ionic strengths.

SPR. To investigate the pH switching behavior of the CP grafted brushes further, surface plasmon resonance (SPR) measurements were performed. Conductive polymers commonly have a high refractive index (generally exhibiting both a real (n) and imaginary part (κ)), which is also dependent on the oxidation state of the polymer.[68] It is therefore necessary to analyze very thin films of CPs by SPR. To produce thin and homogeneous films, we utilized a purpose-made simple PDMS chamber with a built-in counter and reference electrode. This chamber was sealed against the SPR chip using clamps and filled up with polymerization solution. The strict geometry imposed in the setup and the removal of any effects from the liquid meniscus, by simply using a horizontal arrangement, allowed the production of PBrEDOT films suitable for SPR with a thickness in the range of 6−20 nm. Modeling of the SPR curves after grafting of the brushes is complex due to the distinct layers present, but initial modeling reveal a 15 nm thick layer of PAA (modeled in water with $n_{PAA} = 1.35$) on top of an 18 nm thick CP layer. Figure 8 shows SPR data of PBrEDOT-*g*-PAA and the ungrafted control (PBrEDOT). From Figure 8A it is evident that PBrEDOT-*g*-PAA is pH sensitive, in accordance with cyclic voltammetry results (Figure 7A). Milli-Q water adjusted to pH ≈10 or pH ≈4 by addition of acid or base (without addition of salt or buffering agent) was introduced using the flow cell. The data in Figure 8A have been normalized to the same starting value and baseline corrected in the case of PBrEDOT-*g*-PAA (the original data are available in the Supporting Information (Figure S9)). When the surface is exposed to acidic water (pH 4), a steep increase in resonant angle is seen for the grafted sample (Figure 8A), whereas there was a minimal response of the control sample toward pH. The increase in resonant angle upon exposing the sample to acidic pH is interpreted as a collapse of the PAA brushes, leading to a decreased thickness of the layer and a subsequent increase in the refractive index of the PAA brushes. The resonant angle changes as a consequence of changes in either film thickness or film refractive index. A reduction in film thickness would be expected to lead to a reduction in resonant angle, while an increase in refractive index should lead to an increase in resonant angle. It has previously been demonstrated that PAA brushes lead to a decrease in resonant angle upon collapse, interpreted as mainly a thickness related effect.[57,58] Sarkar et al.[58] further identified the respective contributions from thickness and refractive index related effects to the SPR response upon collapse/swelling of PAA brushes. Here, we see an increase in resonant angle upon reduction of pH and thus interpret this as mainly a refractive index effect. We attribute the difference compared to literature to differences in experimental conditions, such as the presence of the CP layer and the grafting time (considerably shorter in our case).

To investigate if applying a potential to the film brings about any changes of the film morphology, in-situ electrochemical SPR experiments were performed where the SPR chip constitutes the working electrode of an electrochemical cell coupled to a potentiostat (ionic strength of 50 mM NaCl, pH 4 or 9). The potential was held at 0.4, 0, or −0.25 V while the SPR curves were recorded. In Figure 8B, the normalized change in resonant angle over time is presented for the grafted and ungrafted sample at basic or acidic pH. The conducting polymer film itself exhibits a large response to the applied potential as the oxidation state of the polymer changes the refractive index of the polymer, as expected.[68] To account for slightly different film thicknesses of the PBrEDOT, the data presented are normalized in several ways. For visualization, the data are adjusted to start at 0° and cut to overlay in time. Furthermore, the data are normalized to the jump between 0 and −0.25 V to account for the difference in film thickness of the conductive polymer layer (the original data are presented in Figure S9). As only the change in resonant angle is presented here, changes in the light absorption of the films are not taken into account (such changes moves the SPR curve up and down rather than shifting the value of the resonant angle),[65] but only the CP exhibits changes to the imaginary part of the refractive index, while the PAA brushes do not absorb light.[69] In Figure 8B, a slow increase in the resonant angle can be seen upon oxidation of the PBrEDOT-*g*-PAA film (0.4 V) if the film is in a basic aqueous environment (i.e., with deprotonated, charged, and extended brushes); no such slow dynamic is seen for the control or for PBrEDOT-*g*-PAA in an acidic environment (i.e., with protonated, uncharged, and collapsed brushes). As previously discussed, the PBrEDOT-*g*-PAA polymer appears to be cation doped at basic pH, leading to cations being expelled from the film during oxidation (Figure 8C provides an illustration of the proposed changes to the layers). The large electrostatic energy of the charged PAA brushes contributes to make such a process slow. Similar effects from electrochemical SPR have been reported for polyaniline and poly(acrylic acid) composite films;[68] however, the effect was interpreted as a swelling of the composite film (consistent with anion uptake). We associated an increase in resonant angle with collapse of the brushes in the case of changing the pH (Figure 8A). Thus, we suggest that the extended grafted poly(acrylic acid) brushes are undergoing some level of conformational collapse when the polymer is oxidized, while at pH 4 the brushes are already collapsed prior to polymer oxidation. Upon oxidation of the polymer and expulsion of cations, the negatively charged PAA brushes may undergo a conformational change to balance the charge of the oppositely charged CP.

In conclusion, we have made a novel conducting polymer with sites for grafting from. We present conditions for electropolymerization of the modified monomer and its copolymerization with EDOT onto large electrodes. The novel conducting polymer, here termed PBrEDOT, was characterized carefully; we present both CVs and assigned Raman and FT-IR spectra. Polymer films containing the ATRP-initiating site were subsequently grafted with *tert*-butyl acrylate and converted to poly(acrylic acid) brushes. The grafted conductive polymer films exhibit pH sensitivity and improved redox processes at basic pH due to the improved solubility of the polymer in aqueous solution derived from the extended poly(acrylic acid) brushes. SPR data support that the brushes collapse upon exposure to acidic pH and indicated electrochemical modulation of the brush conformation at high pH, interpreted as an effect of the charged brushes functioning as a dopant for the conductive polymer. Poly(acrylic acid) is a promising biointerface material. It provides sites for bioconjugation as well as reduced nonspecific interactions with protein in its extended negatively charged state.[70] The improved redox behavior of the grafted polymer in aqueous solution shows potential for applications as a functional biointerface and by conjugating the brushes with peptides or proteins the system would provide a versatile cell culture substrate. Carboxylic acid functionalized PEDOT has also been shown to be a useful substrate for DNA-based biosensors,[71−73] a property that may be further improved upon by multiplexing of the carboxylic acid coupling sites such as herein.

■ ASSOCIATED CONTENT

Ⓢ Supporting Information

We present supporting figures of electrochemistry of PEDOT, PBrEDOT, XPS assignments, full Raman and FT-IR spectra, FT-IR of PBrEDOT-*g*-PS, full FT-IR spectra of PBrEDOT-*g*-PAA and polyacrylate reference spectra, cyclic voltammetry of PBrEDOT-*g*-PAA at additional salt concentrations, and unmodified SPR data; tables presenting elemental composition from XPS and assignments of Raman and FT-IR. This material is available free of charge via the Internet at http://pubs.acs.org.

■ AUTHOR INFORMATION

Corresponding Author

*E-mail: j.malmstrom@auckland.ac.nz (J.M.); j.travas-sejdic@auckland.ac.nz (J.T-S.).

Notes

The authors declare no competing financial interest.

■ ACKNOWLEDGMENTS

The authors acknowledge the help from Dr Colin Doyle for acquiring the XPS data, Shane Crump for help with infrared spectroscopy and Paul Baek for assistance with electrochemical testing. Funding from University of Auckland (Faculty of Science Research Development Fund) is gratefully acknowledged, as is the instrument loan and consumables supplied by BioNavis Ltd.

■ REFERENCES

(1) Bendrea, A. D.; Cianga, L.; Cianga, I. *J. Biomater. Appl.* **2011**, *26*, 3−84.
(2) Quigley, A. F.; Razal, J. M.; Thompson, B. C.; Moulton, S. E.; Kita, M.; Kennedy, E. L.; Clark, G. M.; Wallace, G. G.; Kapsa, R. M. I. *Adv. Mater.* **2009**, *21*, 4393−+.
(3) Chen, C. S.; Mrksich, M.; Huang, S.; Whitesides, G. M.; Ingber, D. E. *Science* **1997**, *276*, 1425−1428.
(4) Lutolf, M. P.; Gilbert, P. M.; Blau, H. M. *Nature* **2009**, *462*, 433−441.
(5) Sano, S.; Kato, K.; Ikada, Y. *Biomaterials* **1993**, *14*, 817−822.
(6) Cole, M. A.; Voelcker, N. H.; Thissen, H.; Griesser, H. J. *Biomaterials* **2009**, *30*, 1827−1850.
(7) Mendes, P. M. *Chem. Soc. Rev.* **2008**, *37*, 2512−2529.
(8) Wischerhoff, E.; Uhlig, K.; Lankenau, A.; Borner, H. G.; Laschewsky, A.; Duschl, C.; Lutz, J. F. *Angew. Chem., Int. Ed.* **2008**, *47*, 5666−5668.
(9) Yeung, C. L.; Iqbal, P.; Allan, M.; Lashkor, M.; Preece, J. A.; Mendes, P. M. *Adv. Funct. Mater.* **2010**, *20*, 2657−2663.
(10) Liu, F.; Urban, M. W. *Prog. Polym. Sci.* **2010**, *35*, 3−23.
(11) Lahann, J.; Mitragotri, S.; Tran, T.-N.; Kaido, H.; Sundaram, J.; Choi, I. S.; Hoffer, S.; Somorjai, G. A.; Langer, R. *Science* **2003**, *299*, 371−374.
(12) Wallace, G.; Spinks, G. *Soft Matter* **2007**, *3*, 665−671.
(13) Pron, A.; Rannou, P. *Prog. Polym. Sci.* **2002**, *27*, 135−190.
(14) Higgins, M. J.; Molino, P. J.; Yue, Z. L.; Wallace, G. G. *Chem. Mater.* **2012**, *24*, 828−839.
(15) Svennersten, K.; Larsson, K. C.; Berggren, M.; Richter-Dahlfors, A. *Biochim. Biophys. Acta, Gen. Subj.* **2011**, *1810*, 276−285.
(16) Wallace, G. G.; Moulton, S. E.; Clark, G. M. *Science* **2009**, *324*, 185−186.
(17) Wang, X. J.; Berggren, M.; Inganas, O. *Langmuir* **2008**, *24*, 5942−5948.
(18) Asplund, M.; Thaning, E.; Lundberg, J.; Sandberg-Nordqvist, A. C.; Kostyszyn, B.; Inganas, O.; von Holst, H. *Biomed. Mater.* **2009**, *4*, 12.
(19) Ateh, D. D.; Navsaria, H. A.; Vadgama, P. *J. R. Soc. Interface* **2006**, *3*, 741−752.
(20) Durgam, H.; Sapp, S.; Deister, C.; Khaing, Z.; Chang, E.; Luebben, S.; Schmidt, C. E. *J. Biomater. Sci., Polym. Ed.* **2010**, *21*, 1265−1282.
(21) Kotwal, A.; Schmidt, C. E. *Biomaterials* **2001**, *22*, 1055−1064.
(22) Molino, P. J.; Higgins, M. J.; Innis, P. C.; Kapsa, R. M. I.; Wallace, G. G. *Langmuir* **2012**, *28*, 8433−8445.
(23) Braunecker, W. A.; Matyjaszewski, K. *Prog. Polym. Sci.* **2007**, *32*, 93−146.
(24) Chen, T.; Ferris, R.; Zhang, J.; Ducker, R.; Zauscher, S. *Prog. Polym. Sci.* **2010**, *35*, 94−112.
(25) Barbey, R.; Lavanant, L.; Paripovic, D.; Schuwer, N.; Sugnaux, C.; Tugulu, S.; Klok, H.-A. *Chem. Rev.* **2009**, *109*, 5437−5527.
(26) Shen, J.; Masaoka, H.; Tsuchiya, K.; Ogino, K. *Polym. J.* **2008**, *40*, 421−427.
(27) Shen, J.; Ogino, K. *Chem. Lett.* **2005**, *34*, 1616−1617.
(28) Wang, M.; Zou, S.; Guerin, G.; Shen, L.; Deng, K.; Jones, M.; Walker, G. C.; Scholes, G. D.; Winnik, M. A. *Macromolecules* **2008**, *41*, 6993−7002.
(29) Rugen-Penkalla, N.; Klapper, M.; Mullen, K. *Macromolecules* **2012**, *45*, 2301−2311.
(30) Choi, J.; Ruiz, C. R.; Nesterov, E. E. *Macromolecules* **2010**, *43*, 1964−1974.
(31) Costanzo, P. J.; Stokes, K. K. *Macromolecules* **2002**, *35*, 6804−6810.
(32) Economopoulos, S. P.; Chochos, C. L.; Gregoriou, V. G.; Kallitsis, J. K.; Barrau, S.; Hadziioannou, G. *Macromolecules* **2007**, *40*, 921−927.
(33) Grande, C. D.; Tria, M. C.; Jiang, G. Q.; Ponnapati, R.; Advincula, R. *Macromolecules* **2011**, *44*, 966−975.
(34) Kang, E. T.; Tan, K. L.; Liaw, D. J.; Chiang, H. H. *J. Mater. Sci.* **1996**, *31*, 1295−1301.
(35) Mandal, A.; Nandi, A. K. *Macromol. Chem. Phys.* **2011**, *212*, 1636−1647.
(36) Pei, Y.; Travas-Sejdic, J.; Williams, D. E. *Langmuir* **2012**, *28*, 8072−8083.
(37) O'Connell, C. D.; Higgins, M. J.; Nakashima, H.; Moulton, S. E.; Wallace, G. G. *Langmuir* **2012**, *28*, 9953−9960.

(38) Strover, L.; Roux, C.; Malmstrom, J.; Pei, Y. W.; Williams, D. E.; Travas-Sejdic, J. *Synth. Met.* **2012**, *162*, 381−390.
(39) Strover, L. T.; Malmström, J.; Laita, O.; Reynisson, J.; Aydemir, N.; Nieuwoudt, M. K.; Williams, D. E.; Dunbar, P. R.; Brimble, M.; Travas-Sejdic, J. *Polymer* **2013**, *54*, 1305−1317.
(40) Davis, K. A.; Charleux, B.; Matyjaszewski, K. *J. Polym. Sci., Part A: Polym. Chem.* **2000**, *38*, 2274−2283.
(41) Quigley, A. F.; Bulluss, K. J.; Kyratzis, I. L. B.; Gilmore, K.; Mysore, T.; Schirmer, K. S. U.; Kennedy, E. L.; O'Shea, M.; Truong, Y. B.; Edwards, S. L.; Peeters, G.; Herwig, P.; Razal, J. M.; Campbell, T. E.; Lowes, K. N.; Higgins, M. J.; Moulton, S. E.; Murphy, M. A.; Cook, M. J.; Clark, G. M.; Wallace, G. G.; Kapsa, R. M. I. *J. Neural Eng.* **2013**, 10.
(42) Arias-Pardilla, J.; Otero, T. F.; Yu, H. H. *Electrochim. Acta* **2011**, *56*, 10238−10245.
(43) Besbes, M.; Trippe, G.; Levillain, E.; Mazari, M.; Le Derf, F.; Perepichka, I. F.; Derdour, A.; Gorgues, A.; Salle, M.; Roncali, J. *Adv. Mater.* **2001**, *13*, 1249−1252.
(44) Bu, H. B.; Gotz, G.; Reinold, E.; Vogt, A.; Schmid, S.; Blanco, R.; Segura, J. L.; Bauerle, P. *Chem. Commun.* **2008**, 1320−1322.
(45) Bu, H. B.; Gotz, G.; Reinold, E.; Vogt, A.; Schmid, S.; Segura, J. L.; Blanco, R.; Gomez, R.; Bauerle, P. *Tetrahedron* **2011**, *67*, 1114−1125.
(46) Guler, F. G.; Gilsing, H. D.; Schulz, B.; Sarac, A. S. *J. Nanosci. Nanotechnol.* **2012**, *12*, 7869−7878.
(47) Spires, J. B.; Peng, H.; Williams, D. E.; Soeller, C.; Travas-Sejdic, J. *Electrochim. Acta* **2010**, *55*, 3061−3067.
(48) Wu, T.; Gong, P.; Szleifer, I.; Vlček, P.; Šubr, V.; Genzer, J. *Macromolecules* **2007**, *40*, 8756−8764.
(49) Morea, G.; Sabbatini, L.; West, R. H.; Vickerman, J. C. *Surf. Interface Anal.* **1992**, *18*, 421−429.
(50) Sakmeche, N.; Aeiyach, S.; Aaron, J. J.; Jouini, M.; Lacroix, J. C.; Lacaze, P. C. *Langmuir* **1999**, *15*, 2566−2574.
(51) Nguyen, T. P.; de Vos, S. A. *Appl. Surf. Sci.* **2004**, *221*, 330−339.
(52) Chiu, W. W.; Travaš-Sejdić, J.; Cooney, R. P.; Bowmaker, G. A. *J. Raman Spectrosc.* **2006**, *37*, 1354−1361.
(53) Garreau, S.; Louarn, G.; Buisson, J. P.; Froyer, G.; Lefrant, S. *Macromolecules* **1999**, *32*, 6807−6812.
(54) Garreau, S.; Louarn, G.; Froyer, G.; Lapkowski, M.; Chauvet, O. *Electrochim. Acta* **2001**, *46*, 1207−1214.
(55) Louarn, G.; Buisson, J. P.; Lefrant, S.; Fichou, D. *J. Phys. Chem.* **1995**, *99*, 11399−11404.
(56) Dong, R.; Lindau, M.; Ober, C. K. *Langmuir* **2009**, *25*, 4774−4779.
(57) Akkahat, P.; Mekboonsonglarp, W.; Kiatkamjornwong, S.; Hoven, V. P. *Langmuir* **2012**, *28*, 5302−5311.
(58) Sarkar, D.; Somasundaran, P. *Langmuir* **2004**, *20*, 4657−4664.
(59) Aulich, D.; Hoy, O.; Luzinov, I.; Brucher, M.; Hergenroder, R.; Bittrich, E.; Eichhorn, K. J.; Uhlmann, P.; Stamm, M.; Esser, N.; Hinrichs, K. *Langmuir* **2010**, *26*, 12926−12932.
(60) Gong, P.; Wu, T.; Genzer, J.; Szleifer, I. *Macromolecules* **2007**, *40*, 8765−8773.
(61) Kurosawa, S.; Aizawa, H.; Talib, Z. A.; Atthoff, B.; Hilborn, J. *Biosens. Bioelectron.* **2004**, *20*, 1165−1176.
(62) Kim, B. S.; Chen, L.; Gong, J. P.; Osada, Y. *Macromolecules* **1999**, *32*, 3964−3969.
(63) Thompson, B. C.; Richardson, R. T.; Moulton, S. E.; Evans, A. J.; O'Leary, S.; Clark, G. M.; Wallace, G. G. *J. Controlled Release* **2010**, *141*, 161−167.
(64) Ali, E. M.; Kantchev, E. A. B.; Yu, H. H.; Ying, J. Y. *Macromolecules* **2007**, *40*, 6025−6027.
(65) Breukers, R. D.; Gilmore, K. J.; Kita, M.; Wagner, K. K.; Higgins, M. J.; Moulton, S. E.; Clark, G. M.; Officer, D. L.; Kapsa, R. M. I.; Wallace, G. G. *J. Biomed. Mater. Res., Part A* **2010**, *95A*, 256−268.
(66) Lego, B.; Skene, W. G.; Giasson, S. *Macromolecules* **2010**, *43*, 4384−4393.
(67) Moulton, S. E.; Higgins, M. J.; Kapsa, R. M. I.; Wallace, G. G. *Adv. Funct. Mater.* **2012**, *22*, 2003−2014.
(68) Wallace, G. G.; Higgins, M. J.; Moulton, S. E.; Wang, C. *Nanoscale* **2012**, *4*, 4327−4347.
(69) Bittrich, E.; Kuntzsch, M.; Eichhorn, K. J.; Uhlmann, P. *J. Polym. Sci., Part B: Polym. Phys.* **2010**, *48*, 1606−1615.
(70) Rastogi, A.; Nad, S.; Tanaka, M.; Da Mota, N.; Tague, M.; Baird, B. A.; Abruna, H. D.; Ober, C. K. *Biomacromolecules* **2009**, *10*, 2750−2758.
(71) Thompson, B. C.; Chen, J.; Moulton, S. E.; Wallace, G. G. *Nanoscale* **2010**, *2*, 499−501.
(72) Luo, S. C.; Xie, H.; Chen, N. Y.; Yu, H. H. *ACS Appl. Mater. Interfaces* **2009**, *1*, 1414−1419.
(73) Peng, H.; Zhang, L.; Soeller, C.; Travas-Sejdic, J. *Biomaterials* **2009**, *30*, 2132−2148.